

非結晶碳於複晶矽雷射再結晶之應用

研究生：高德倫

指導教授：冉曉雯 博士

國立交通大學

顯示科技研究所碩士班

摘要

複晶矽薄膜電晶體的效能受到元件通道中的晶粒邊界 (Grain Boundaries, GBs) 劇烈影響，這些晶粒邊界會降低載子遷移率並增加元件關閉狀態下的漏電流。為了降低以上的效應，我們利用外加的熱儲存層 (H-REC)，來加大雷射退火後的晶粒尺寸，以減少元件通道中的晶界數量。首先，我們使用數值分析的方法來模擬雷射結晶時，熱流在薄膜中流動的情形。並藉由有限元素分析軟體 (Femlab) 來計算熱能於材料中隨時間之流動狀況，我們改變熱儲存層的吸收係數、組成成分以及結構，在不同的雷射能量下來模擬雷射退火的過程。因此，我們可以找出雷射退火結晶的最佳狀況。

含氫之非晶碳膜(a-C:H)在寬廣的波段中顯示出非常高的光學吸收性。可在許多的雷射退火機台上做為熱儲存層材料，如：準分子雷射(351nm)與固態雷射(532nm)。在研究中，我們以 XeF 準分子雷射搭配 a-C:H 熱儲存層，進行複晶矽雷射結晶。由於熱儲存層的加入，複晶矽融熔時間將因而大幅度的提升，並且可成長出較大的晶粒。而由拉曼光譜分析，最佳化的峰值的位置及半高寬分別為 516.7 cm^{-1} 和 3.51 cm^{-1} 。由電子顯微鏡的圖像可發現外加儲熱層的矽膜具有較大的晶粒。此外，拉曼分析在本論文中亦將被用來討論 a-C:H 被雷射退火之後的鍵結改變。

The Application of Amorphous Carbon on Poly Silicon Laser Crystallization

Student: Te-Lun Kao

Advisors: Dr. Hsiao-Wen Zan

Institute of Display

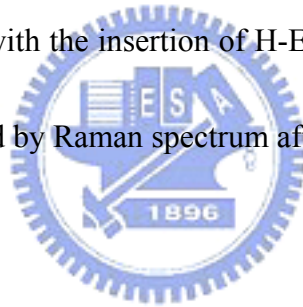
National Chiao Tung University

Abstract

Grain boundaries(GBs) in channel region will influence the poly-Si TFT performance severely, GBs will lower the carrier mobility and increase the off state leakage-current. In order to reduce these effects, we utilized an additional heat retaining enhanced crystallization (H-REC) layer to enlarge the grain size, which can reduce the numbers of GBs in channel region. First, we use the numerical analysis to simulate the heat flux inside the thin film during laser crystallization. With the aid of the software of finite element modeling laboratory (FEMLAB), we change the heat absorption coefficient, components, and structure of the H-REC layer to model the process of laser annealing under different laser intensity. Hence, we can find out the optimized condition for laser recrystallization.

The hydrogen contained amorphous carbon film (a-C:H) shows a highly

absorbent property during a wide wavelength. It can be used as an H-REC layer in several process of laser recrystallization, such as excimer laser (351nm) and solid state laser (532nm). In this study, we utilized the XeF excimer laser and the a-C:H film as the H-REC layer to process the experiment of poly-Si laser recrystallization. With the insertion of H-REC layer, the melting time of Si film and the grain size will be prolonged and enlarged, respectively. The optimized poly-Si signal of Raman spectrum, is at 516.7 cm^{-1} and the full width at half maximum (FWHM) is 3.51 cm^{-1} . From the scanning electron microscope (SEM) images, it is found that the larger poly-Si grains will appear with the insertion of H-ERC layer. Besides, the change of a-C:H layer is also analyzed by Raman spectrum after the laser irradiation.



致謝

在這兩年的碩士生涯中，成長了很多。首先，我要感謝我的指導教授：冉曉雯博士。兩年來她不僅對我的研究細心的指導，在人生态度上也給了我很多的建議，在此致上最誠摯的謝意。

並且我要感謝國錫學長、政偉學長、士欽學長、貞儀學姊，在這兩年來的幫助與鼓勵。尤其是政偉學長，在我最後一年來的研究生涯裡，用心的教導我且辛苦地協助我完成我的碩士論文。感謝清大的坤益學長以及建佑學弟，這一年來辛苦的幫我沉積碳膜。感謝一起做實驗、一起討論、一起歡笑的同學：育敏、而康、廷遠、皇維、光明、睿志、俊德。

最後，我要感謝我的家人對我的支持以及照顧，在我開心時和我分享我的喜悅以及在我最失意的時候扶持我鼓勵我，沒有你們，就不會有今日的我。

高德倫 2007年9月 於國立交通大學



Contents

Chinese Abstract	I
English Abstract	II
Acknowledgment	IV
Contents	V
Table Captions	VII
Figure Captions	VIII
Chapter 1 Introduction	
1.1 Background and overview of low temperature poly-Si (LTPS) TFTs technology	1
1.2 Introduction of amorphous carbon (a-C:H)	5
1.3 Motivation	6
Chapter 2 Fabrication process and Heat Flux Simulation	
2.1 Thin film deposition	7
2.1.2 Silicon oxide formation	7
2.1.2 a -C:H film formation	7
2.1.3 Amorphous silicon formation	7
2.2 Material analysis	8
2.2.1 The absorption coefficient (α)	8
2.2.2 SEM	9
2.2.3 Raman spectrum	9
2.3 Heat flux analysis	10
Chapter 3 Result and Discussion	
3.1 Excimer laser crystallization with the heat retain layer (HRL) - a-C:H	13
3.1.1 The absorption coefficient of a-C:H film	13

3.1.2 The heat flux analysis of the silicon crystallized on different HRL	13
3.2 Raman analysis	16
3.2.1 Raman analysis of the crystallized poly-si film	16
3.2.2 Raman analysis of the a-C:H film	17
Chapter 4 Conclusion	19
Reference	21
Table	25
Figures	27



Table Captions

- Table I** Thermal conductivity, density, specific heat and other parameters used in the simulation. The value of absorption coefficient was measured by n&k analyzer.
- Table II** The absorption coefficient of a-C:H film which deposits in different condition. The wave length of laser (a) $\lambda = 308 \text{ nm}$ (b) $\lambda = 532 \text{ nm}$
- Table III** (a) The $I(G)/I(D)$ of a-C:H film before and after laser irradiated
(b) Thermal conductivity, density, and other heat capacity of sp^2 -band and sp^3 - band.
- Table IV** The X_c (crystalline volume factor) of (a) sample A and (b) sample B with different laser energy density



Figure Captions

Chapter 1

Fig.1-1-1 (a) fabrication procedure combining MILC and ELA with a pit structure

(b) SEM image with laser energy = 733mJ/cm^2 (c) SEM image with

laser energy = 775 mJ/cm^2 .

Fig.1-1-2 According to the laser energy density, the crystallization could be

discussed into three regimes: (a) partially melting fluence, (b)

completely melting fluence, (c) super lateral growth (SLG).

Fig.1-1-3 The relation between the laser fluence and the grain size.

Chapter 2

Fig. 2-2-1 The absorptivity of a-C:H film. The thickness of DLC is 100nm.

Fig. 2-2-2 The Raman spectra of the carbon film

Fig. 2-3-1 The left part of picture is the normal meshes in the structure and the right part is the refined meshes in the structure. The refine meshes would increase the accuracy of the final result.

Fig. 2-3-2 The structure for simulation, the top layer is α -Si ,the middle lay is a-C:H ,and the bottom layer is SiO₂. The dimensions and the boundary conditions of each side are labeled on it.

Fig. 2-3-3 (a) Thermal distribution at a certain time = 800 ns, (b) the contour lines of the heat flux at a certain time = 800ns (c) Temperature curve of a particular point ($1.5\mu\text{m}$, $1.15\mu\text{m}$) versus the time (d) Temperature curve versus the position of y at different time (at 20ns, 50ns, 100ns, and 200ns)

Chapter 3

Fig. 3-1-1 (a) The cross section of the structure (b) The temperature curve versus the time with different laser energy (c) The latent heat time versus the laser energy

Fig. 3-1-2 (a) The temperature curve versus the time with different absorption coefficient (b) The latent heat time versus the absorption coefficient.

Fig. 3-1-3 (a) The a-C:H film deposit on the SiO₂, and then the a-Si deposit on a-C:H film without pattern. (b) a-C:H with pattern (c) a-Si with pattern (d) The temperature curve versus the time with different structures.

Fig. 3-1-4 (a) The cross-section of sample A (b) The cross-section of sample B

Fig. 3-1-5 SEM image of sample (a) A with laser energy density of 175 mJ/cm^2 (b) B with laser energy density of 175 mJ/cm^2 (c) A with laser energy density of 200 mJ/cm^2 (d) B with laser energy density of 200 mJ/cm^2 (e) A with laser energy density of 225 mJ/cm^2 (f) B with laser energy density of 225 mJ/cm^2 (g) A with laser energy density of 250 mJ/cm^2 (h) B with laser energy density of 250 mJ/cm^2 (i) A with laser energy density of 275 mJ/cm^2 (j) B with laser energy density of 275 mJ/cm^2 (k) A with laser energy density of 300 mJ/cm^2 (l) B with laser energy density of 300 mJ/cm^2 (m) A with laser energy density of 350 mJ/cm^2 (n) B with laser energy density of 350 mJ/cm^2 (o) A with laser energy density of 400 mJ/cm^2 (p) B with laser energy density of 400 mJ/cm^2

Fig. 3-2-1 The Raman spectra of sample A with laser energy density of (a) 175 mJ/cm^2 (b) 200 mJ/cm^2 (c) 250 mJ/cm^2 (d) 300 mJ/cm^2 (e)

350mJ/cm²

Fig. 3-2-2 The Raman spectra of sample B with laser energy density of (a) 175 mJ/cm²(b) 200 mJ/cm²(c) 250 mJ/cm²(d) 300 mJ/cm² (e)350mJ/cm²

Fig. 3-2-3 (a) FWHM of sample A with laser energy density of 175 mJ/cm² ~ 350 mJ/cm² (b) peak position of sample A with laser energy density of 175 mJ/cm² ~ 350 mJ/cm²

Fig. 3-2-4 (a) FWHM of sample B with laser energy density of 175 mJ/cm² ~ 350 mJ/cm² (b) peak position of sample B with laser energy density of 175 mJ/cm² ~ 350 mJ/cm².

Fig.3-2-5 The Raman spectrum of a-C:H before and after laser irradiated by 100 to 400mJ/cm²

